PLoS one

Oscillatory Dynamics of Cell Cycle Proteins in Single Yeast Cells Analyzed by Imaging Cytometry

David A. Ball[1], Julie Marchand[1], Magaly Poulet[1], William T. Baumann[2], Katherine C. Chen[3], John J. Tyson[3], Jean Peccoud[1,4]*

1 Virginia Bioinformatics Institute, Virginia Tech, Blacksburg, Virginia, United States of America, 2 Department of Electrical and Computer Engineering, Virginia Tech, Blacksburg, Virginia, United States of America, 3 Department of Biological Sciences, Virginia Tech, Blacksburg, Virginia, United States of America, 4 Institute for Critical Technology and Applied Science Center for Systems Biology of Engineered Tissues, Virginia Tech, Blacksburg, Virginia, United States of America

Abstract

Progression through the cell division cycle is orchestrated by a complex network of interacting genes and proteins. Some of these proteins are known to fluctuate periodically during the cell cycle, but a systematic study of the fluctuations of a broad sample of cell-cycle proteins has not been made until now. Using time-lapse fluorescence microscopy, we profiled 16 strains of budding yeast, each containing GFP fused to a single gene involved in cell cycle regulation. The dynamics of protein abundance and localization were characterized by extracting the amplitude, period, and other indicators from a series of images. Oscillations of protein abundance could clearly be identified for Cdc15, Clb2, Cln1, Cln2, Mcm1, Net1, Sic1, and Whi5. The period of oscillation of the fluorescently tagged proteins is generally in good agreement with the inter-bud time. The very strong oscillations of Net1 and Mcm1 expression are remarkable since little is known about the temporal expression of these genes. By collecting data from large samples of single cells, we quantified some aspects of cell-to-cell variability due presumably to intrinsic and extrinsic noise affecting the cell cycle.

Introduction

The cell division cycle is the sequence of events whereby a living cell replicates its components and divides them between two daughter cells, so that each daughter receives the information and machinery necessary to repeat the process. Progression through the cell cycle is governed by a complex but precise molecular mechanism relying on checkpoints to ensure that every newborn cell receives one complete set of chromosomes [1]. Although the sequence of events is very tightly controlled, the time taken to progress through each stage of the cell cycle may vary considerably from cell to cell. Modelers have recognized the need to incorporate this cell-to-cell variability into their models, and have started to transform their deterministic models into stochastic versions [2,3]. In a recent paper, we used stochastic modeling and single-cell microscopy to characterize a budding yeast mutant that exhibits stochastic fluctuations between cell division and cell cycle arrest when grown on alternative carbon sources (e.g., raffinose) that support slower growth rates than glucose [4].

Previous research into the expression of genes controlling progression through the eukaryotic cell cycle has heavily relied on bulk measurements, such as western (and northern) blots and micro-arrays, on populations of cells that have been synchronized by some strong perturbation, for examples see the experimental data used in the development of the model of Chen et al [5].

It has been argued that batch-culture synchronization methods are incapable of creating reliably synchronous populations of cells [6,7]. Proponents of these methods point to the vast amounts of microarray data that have been collected to show that, although not perfect, synchronization has revealed many molecular features of the cell cycle that were previously unknown [8,9]. In any case, one thing that Cooper and Spellman do agree on is that synchronization introduces artifacts that can be difficult to judge. In addition, bulk measurements largely ignore subtle differences between individual cells that arise due to molecular noise [10,11]. However, recent advances, such as the introduction of fluorescent proteins optimized for various organisms [12] and the development of automated microscopy, have allowed the community to begin to re-examine this complex gene network at the single-cell level [13–25].

Different groups have used these tools to explore various aspects of the cell cycle in individual yeast cells. For example, Tully et al. used live-cell imaging to examine the role of the anaphase-promoting complex (APC) in cytokinesis by use of GFP fusions of the actomyosin ring component Iqg1 [23]. Fred Cross's group has used live-cell imaging of fluorescently tagged genes to investigate protein dynamics at the G1-S transition [14] and at mitotic exit [22,25]. More commonly, though, fluorescently labeled proteins are used as staging markers indicative of specific events in the cell cycle. Tagging Myo1 for instance facilitates the detection of bud emergence as this protein concentrates in the bud-neck at this particular stage [16]. Such methods have been extremely useful in determining the roles that noise plays in cell cycle progression [16], and in analyzing how the cell cycle is perturbed in various mutant

strains of budding yeast [15,18,20,21,24]. Rather than using GFP-tagged proteins as timers of cell cycle events in wild-type and mutant cells, we are more interested in their use as reporters of gene expression levels. In this paper, using a representative selection of 16 GFP-tagged cell cycle genes in budding yeast, we provide a broad assessment of the temporal patterns of protein abundance and localization during the cell cycle and of the magnitude of noise affecting these proteins. Using time-lapse microscopy we measured the fluorescence signals of individual cells through 4,835 cell cycles. We developed custom signal processing, data aggregation, and statistical analysis methods to estimate the period, amplitude, and phase of oscillation in the abundance profiles of these 16 cell cycle regulatory proteins. We also monitored the localization of these proteins throughout the cell cycle. Our analysis shows that there are noticeable differences in the noise affecting different proteins. Some appear to be more tightly controlled than others, and all are more noisy than the cell division process itself, suggesting that the cell cycle is somewhat shielded from the fluctuations affecting individual proteins. Examples of both protein abundance and protein localization analyses are shown in Figure 1. We compare our single-cell, single-protein observations with protein dynamics reported in the experimental literature, which are summarized in Table 1. Statistically significant oscillations were observed in the abundance of Net1 and Mcm1, an observation that has not been previously reported in the literature.

Results

Single cell analysis

Protein abundance. First, we tracked the time evolution of cell fluorescence over several cell cycles (Figure 1A). The mean fluorescence of pixels within a cell in a specific frame is used as an indicator of the tagged protein concentration at a particular instant of time. By tracking cells over several frames, it is possible to reconstruct the time evolution of the fluorescence over several cell division cycles spanning several hours. In order to smooth the time-courses of individual cells, non-physiological oscillation frequencies were filtered out of the trajectories. High-frequency noise components with periods of less than 50 minutes, which could originate from sources such as the camera read noise, or segmentation errors, were removed. The unfiltered and filtered time-course of a typical cell for each of the 16 yeast strains are shown in Figure 2, along with a wild-type (WT) control cell not labeled with GFP. The timing of the budding event was manually annotated for each cell and is reported as a black triangle on the x-axis of fluorescence profiles in Figure 2. This series of data extraction and signal processing steps generates a clean signal consistent with some known aspects of cell cycle dynamics. For instance the fluorescence signals collected on the Cln2 and Clb2 tagged strains are well correlated with the cell budding event.

Protein localization. Although a single fluorescently tagged protein cannot be used to unambiguously determine the organelle in which the protein is located, it is possible to determine the area (number of pixels) to which a protein is confined, and how this area changes over time (for example, see Figure 1B). To reduce the effects of organelle motion in and out of focus, these measurements were conducted by collecting images at multiple focal planes for each sample. These multiple focal planes were then combined using a maximum z-projection (see Materials and Methods). To quantify protein localization, we propose an estimator ('pixels above threshold', see Materials and Methods) and plot this estimator as the blue line in Figure 3. The small numbers of pixels above threshold observed for Bck2, Bub2, Cdc15, Esp1, Lte1, Mad2 and Tem1 indicate that these proteins are uniformly distributed throughout the cell, with only a few bright pixels
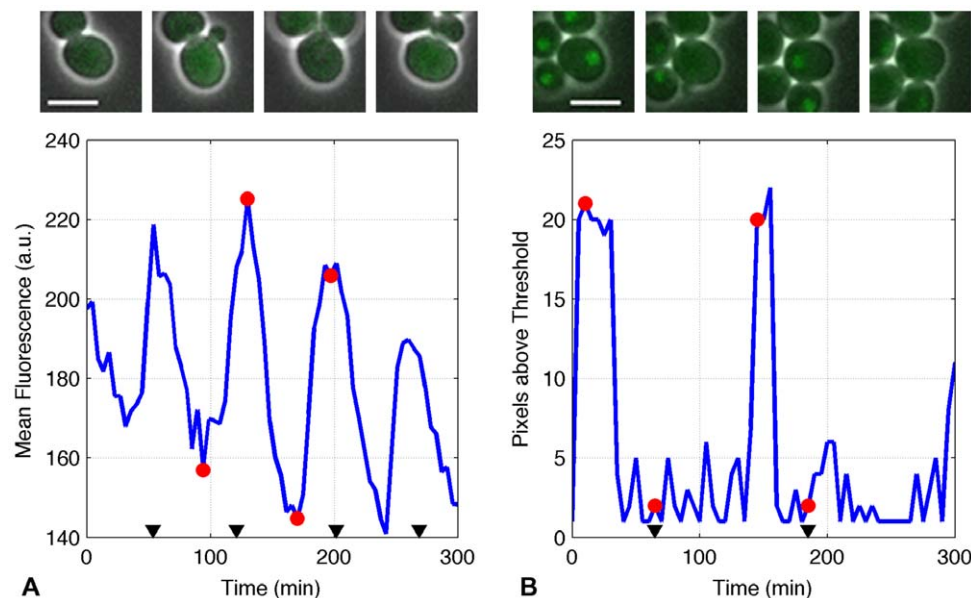

Figure 1. Indicators of protein abundance and protein localization. (A) Comparison between Cln2-GFP images and indication of protein abundance. Here the cell in the center of the image exhibits a noticeable difference in cell fluorescence between images 1 and 3 (low) and images 2 and 4 (high). (B) Comparison between Whi5-GFP images and the indicator of protein localization. On images 1 and 3, when looking at the cell in the center of the images, it is possible to recognize a subcellular structure where more fluorescence is concentrated than in the other regions of the cells. In both parts, the top of the figure shows four images taken over two cell cycles, while the bottom of the figure shows the indicator of protein abundance (A) or fluorescence localization (number of pixels above the threshold) (B). The red circles correspond to the time-points of the four images. The black triangles indicate budding events. The scale bars in the images indicate 5 μm.
doi:10.1371/journal.pone.0026272.g001

Table 1. Known features of proteins involved in the *S. cerevisiae* cell division cycle.

Gene	Protein Role [45]	Protein Localization [43]	Oscillation of mRNA [27]	Mean Number [46]
BCK2	Bck2 is a Cln-independent activator of *CLN1,2* expression [24].	no	no	Not visualized
BUB2	Mitotic exit network regulator blocks cell cycle progression before anaphase in response to spindle misalignment and kinetochore damage.	bud (Anaphase), otherwise spindle-poles [47]	no	Not visualized
CDC6	Component of the pre-replicative complex and a stoichiometric inhibitor of Cdc28-Clb kinase.	cytoplasm (S-phase to end of anaphase), otherwise nucleus [48]	high: late M-phase	Not visualized
CDC15	Protein kinase necessary for mitotic exit.	spindle-poles	no	238
CDC20	Auxiliary component of the anaphase-promoting complex; promotes degradation of Clb's and Pds1.	no	high: M-phase	Not visualized
CLB2	B-type cyclin involved in progression through M phase; accumulates during G2 and M, and is degraded during anaphase and telophase by ubiquitin-mediated proteolysis	nucleus	high: G2	339
CLN1	G1 cyclin involved in the Start transition (late G1) and bud emergence.	no	high: late G1	319
CLN2	G1 cyclin involved in the Start transition (late G1) and bud emergence.	no	high: late G1	1270
ESP1	Separase, a caspase-like cysteine protease that promotes sister chromatid separation by cleaving the cohesin rings that bind sister chromatids together at centromeres	nucleus (metaphase-anaphase transition) [49]	high: S-phase	Low signal
LTE1	LTE1 is essential for termination of M phase at low temperatures, along with TEM1, and CDC15 (5), all part of the mitotic exit network	cytoplasm	no	304
MAD2	Spindle assembly checkpoint protein; sequesters and prevents Cdc20 from activating APC	no	no	1110
MCM1	Transcription factor for Clb2 and Cdc20	nucleus	no	8970
NET1	Core subunit of the RENT complex, which is involved in nucleolar silencing and telophase exit	nucleolus	no	1590
SIC1	Inhibitor of Cdc28-Clb kinase complexes, active in G1 phase	no	high: end of mitosis & G1	768
TEM1	GTPase component of the mitotic exit network [1]	spindle pole	high: G2	573
WHI5	Repressor of G1 transcription, binds to SCB binding factor (SBF) in early G1	nucleus (late mitosis) leaves during G1 [19]	high: S-phase	1440

doi:10.1371/journal.pone.0026272.t001

located next to each other by chance. The patterns observed for Mcm1 and Net1 indicate that these proteins remain extremely localized throughout the cell cycle. Cdc6, Cdc20, Clb2, Sic1, and Whi5 exhibit a couple of sharp bursts over a period of 300 min. In other words, these proteins are distributed evenly throughout the cell volume during most of the cell cycle except during a short period of time (once per cycle), when they concentrate in one location in the cell.

The red plots on Figure 3 report the mean cell fluorescence as described above except that it is computed over 20 focal planes. For some proteins (Cdc6, Clb2, Cln2, Sic1), subtle correlations between changes of protein abundance and protein localization can be observed while the changes of localization observed for Cdc20 and Whi5 occur without any observable changes of protein abundance. Net1 and Mcm1 exhibit complex asymmetric patterns indicating a slow accumulation of protein followed by very rapid decrease in protein abundance.

Unfortunately, the increased light exposure resulting from the observation of multiple focal planes negatively impacted cell growth. As a result only a few cells for each cell line could be observed. It has not been possible to properly assess the fluctuation of protein localization statistics from these small samples.

Population-level statistics

In order to characterize the stochastic dynamics of the cell cycle, we observed 4,835 individual cell cycles and reduce this large data set by extracting the amplitude and period of the fluorescence signals and its relation to budding times. The statistical distribution of these random variables is likely to provide an indication of the global structure of the noise affecting the cell cycle.

Budding events. To determine if the fusion of GFP to any of the investigated proteins was detrimental to the function of that protein, we characterized the division times of each cell by calculating the time between budding events for mother cells (inter-bud time),

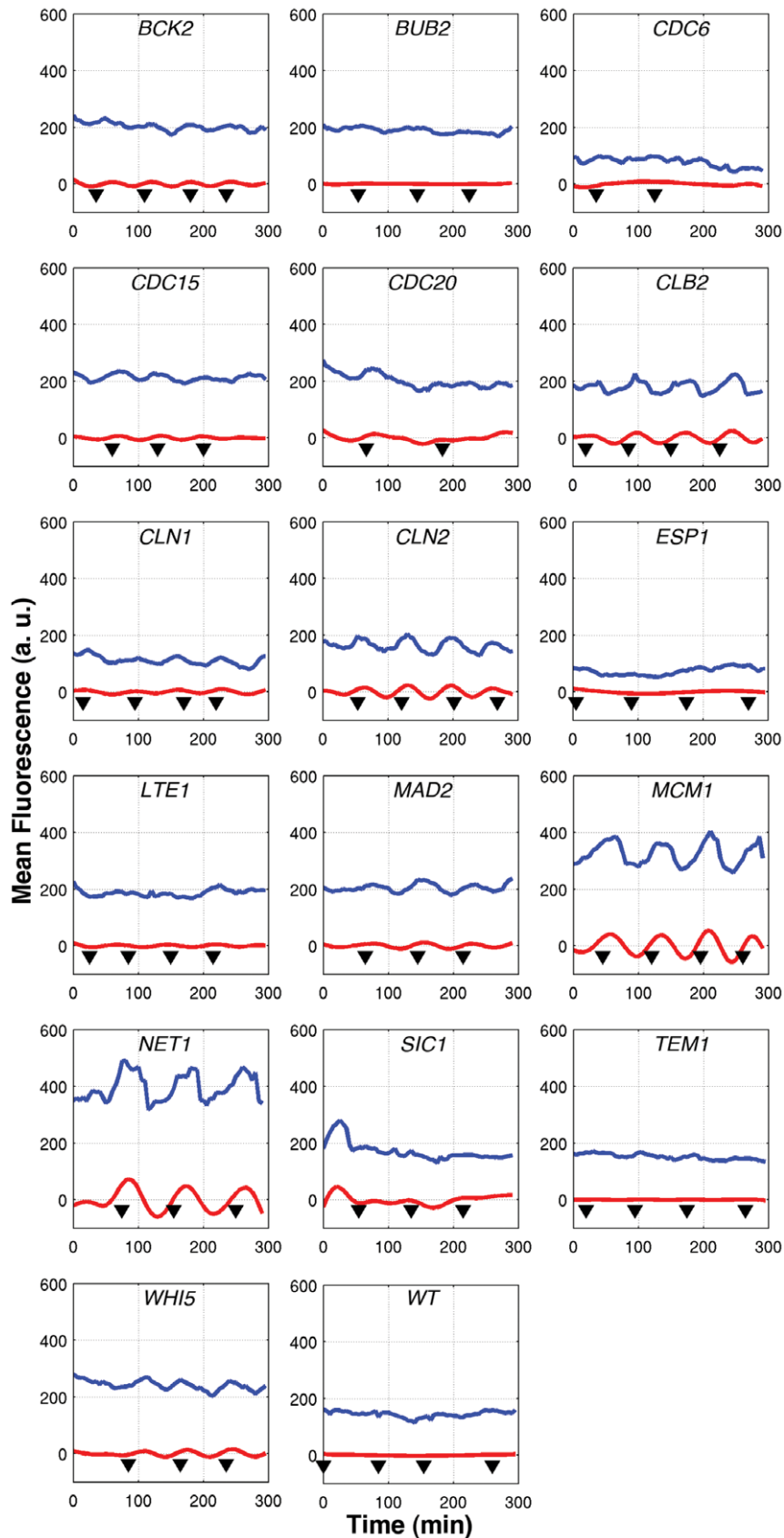**Figure 2. Mean cell fluorescence for individual cells.** The measured mean fluorescence is plotted (blue line) along with the filtered signal (red line) for a single cell expressing GFP as a fusion with the indicated cell-cycle regulator. Filtering removes all high-frequency noise, as well as the DC offset, leaving signals that have a zero mean. Budding events are indicated by black triangles.
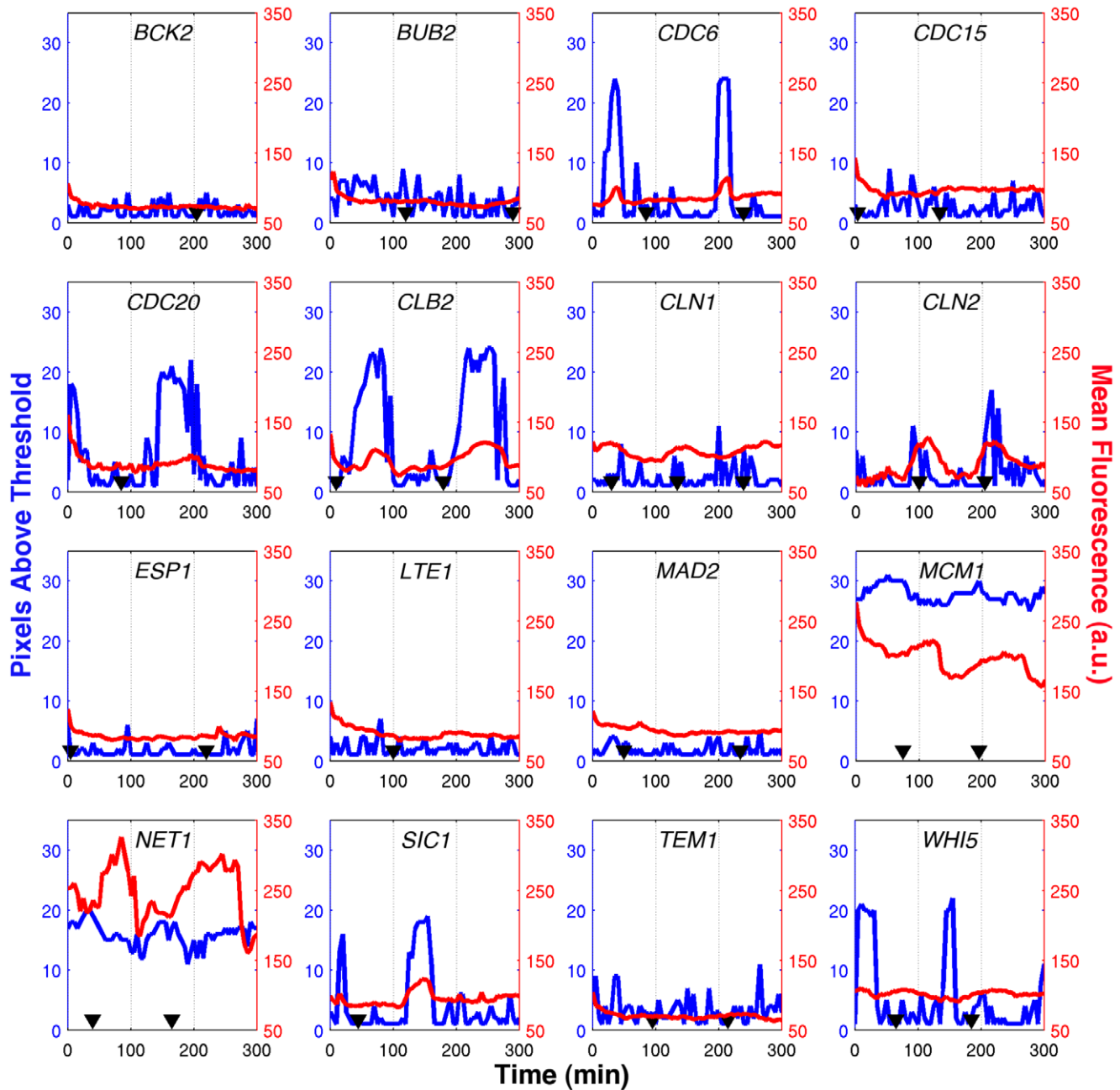doi:10.1371/journal.pone.0026272.g002

Figure 3. Localization of GFP-tagged proteins. Z-stacks of cells expressing a GFP fusion of the indicated protein were projected to a single image and analyzed to determine changes in localization through the cell cycle. The number of connected pixels within the 95th percentile (blue curve) was used as a metric to calculate the degree of localization, with a higher number indicating a larger area of bright pixels. A typical cell from each strain is shown, along with that cell's mean fluorescence over the entire cell (red curve) and the manually annotated budding events (black triangles). Note that the increased light exposure (~20×) resulted in much slower cell-division compared to the single-plane experiments described.
doi:10.1371/journal.pone.0026272.g003

and the time from a daughter's emergence as a bud to its first bud (birth-to-bud time) for each of the strains (Table 2). For most of the strains in this study, the observed cell cycle distributions agree well with each other as well as with the distributions of wild-type cells reported in the literature for both mothers and daughters [5]. With an inter-bud time of 132.2 min compared to 90.0 min for the WT, the *CDC20-GFP* strain is the only one that exhibits a noticeable phenotypic effect that may result from an alteration of the function of the Cdc20 protein by GFP tagging. Hence, we do not include Cdc20 in our further analysis of protein fluctuations.

Protein abundance in absolute time. The dynamics of the mean fluorescence observed on individual cells was characterized by using the peak-to-peak times of the filtered fluorescence signal to measure the period of fluorescence fluctuations, and the difference between the maximum and minimum fluorescence values to determine the amplitude of fluorescence fluctuations. The period and amplitude of fluorescence oscillations were aggregated over multiple cell cycles collected over several individual cells, and are shown in Figure 4. The medians and coefficients of variation of the

Table 2. Extracted oscillation parameters and statistics of inter-bud times (mothers), and birth-to-bud times (daughters) for GFP fusions of the indicated proteins.

tagged gene	# cycles	Amplitude		Protein vs. WT	Period (min)		Mother inter-bud times			Daughters birth-to-bud times		
		Median	CV	p-value (t-test)	Median	CV	# cycles	Median	CV	# cycles	Median	CV
BCK2	211	13.48	0.83	0.046	64.99	0.50	139	74.99	0.26	109	109.99	0.25
BUB2	242	12.59	0.75	0.133	75.00	0.42	125	80.00	0.28	105	110.01	0.24
CDC6	93	11.47	0.94	0.434	85.01	0.52	83	80.01	0.30	65	105.01	0.29
CDC15*	125	17.77	0.73	<0.0001	75.00	0.48	129	75.00	0.19	85	100.00	0.27
CDC20*	26	20.07	0.66	<0.0001	85.16	0.42	20	132.23	0.22	21	129.98	0.20
CLB2*	254	29.78	0.47	<0.0001	80.29	0.32	111	80.29	0.32	101	100.36	0.22
CLN1*	185	19.33	0.60	<0.0001	79.99	0.29	96	84.99	0.26	80	109.99	0.22
CLN2*	63	39.99	0.46	<0.0001	80.68	0.46	64	80.68	0.28	56	118.78	0.20
ESP1	95	13.22	0.96	0.071	90.00	0.41	100	85.00	0.24	70	120.00	0.26
LTE1	69	13.42	0.83	0.049	90.00	0.51	103	80.00	0.25	67	105.00	0.26
MAD2	81	11.17	0.80	0.954	75.00	0.41	56	85.00	0.39	43	115.01	0.27
MCM1*	467	65.33	0.41	<0.0001	75.27	0.34	181	75.27	0.27	151	105.38	0.24
NET1*	114	74.87	0.93	<0.0001	80.00	0.32	53	80.00	0.24	43	115.01	0.18
SIC1*	58	34.08	0.90	<0.0001	105.01	0.48	60	80.00	0.37	50	112.51	0.27
TEM1	53	14.38	0.83	0.687	74.98	0.52	31	79.98	0.29	24	117.47	0.37
WHI5*	129	29.30	0.56	<0.0001	80.00	0.48	64	75.00	0.22	67	105.00	0.26
WT	107	11.83	0.97	1	84.98	0.41	138	89.98	0.31	116	99.97	0.26

*Genes with fluorescence oscillations statistically different from the WT.

mean fluorescence period and amplitude for all the 17 strains are reported in Table 2.

The joint distributions of amplitudes and periods can be represented by heat maps that give a visual indication of the variability of protein abundance over hundreds of cell cycles (Figure 4). This figure highlights the differences in the noise affecting the dynamics of these 16 proteins. For Bub2, Clb2, Cln1, and Mad2, the fluctuations of the period and amplitude are narrowly controlled. In other cases, one parameter is better controlled than the other. Mcm1 and Net1 have narrow period distributions but much wider amplitude distributions whereas Bck2, Cdc6, Cdc15, Cln2, Esp1, Lte1, Tem1, and Whi5 have a narrow amplitude distribution but a wider period distribution. Finally, Sic1 exhibits broad fluctuations of both period and amplitude of fluorescence oscillations. Since these plots correspond to experiments that were conducted on different days with different cell cultures, it is possible that the differences observed reflect some uncontrolled experimental parameters. In order to rule out this possibility, all strains were profiled twice several months apart, and the results were qualitatively similar even though quantitative differences were observed.

To determine whether a GFP-tagged protein is exhibiting statistically significant oscillations in abundance during the cell cycle, we use an unequal variance t-test to compare the tagged protein's amplitude distribution against the background fluorescence fluctuations observed in the untagged WT strain from which the tagged strains were derived. At the 1% significance level (p-value<0.01 in Table 2), we identify Cdc15, Clb2, Cln1, Cln2, Mcm1, Net1, Sic1, and Whi5 as oscillatory proteins (they are marked with an * in Table 2).

For most of the strains exhibiting oscillatory fluorescence, the period of fluorescence is in good agreement with the mother inter-bud time, which is expected, as the software follows the mother cell. Sic1 is a marginal case. The tagged strain proliferates normally (median inter-bud time of mother cells = 80 min), but the median period of fluorescence oscillations is significantly longer (105 min). We choose to retain Sic1 in our further considerations of oscillatory proteins.

Protein abundance in normalized time. In order to determine the point in the cell cycle that peak expression occurs for each protein, we related fluorescence data to manually annotated budding events used for estimating the inter-bud and birth-to-bud times as described above. However, due to cells growing out of the plane of focus, it is not possible to identify all budding events. The phase of the protein expression was taken as the time between a bud emerging and the closest fluorescence peak. For instance, the distribution of bud-to-peak fluorescence times observed on the CLB2-GFP cell line shows that Clb2 abundance generally peaks roughly one quarter of a cell-cycle after bud emergence (Figure 5A). A similar analysis was performed for eight oscillating genes identified above (Cdc15, Clb2, Cln1, Cln2, Mcm1, Net1, Sic1, and Whi5). Results are reported in Figure 5B as heat maps indicating the distribution of the peak of fluorescence. In this figure, the stages of the cell cycle were determined using the information in [26], with the budding event assumed to occur at the G1-S transition. The data analysis procedure was verified to not introduce any unwanted artifacts by its use on simulated cells with fluorescence trajectories composed of purely white noise (Appendix S1).

It is interesting to compare (Table 3) the distribution of peak fluorescence times with the oscillatory dynamics of mRNA [27–29]. We compare our times of peak protein abundance to the peaks in mRNA levels reported by Gauthier et al [27], as their analyses includes the experiments of Pramila et al [28] as well as Spellman et al [29], and their results are presented in a searchable web database (www.cyclebase.org). Most of the genes we identified
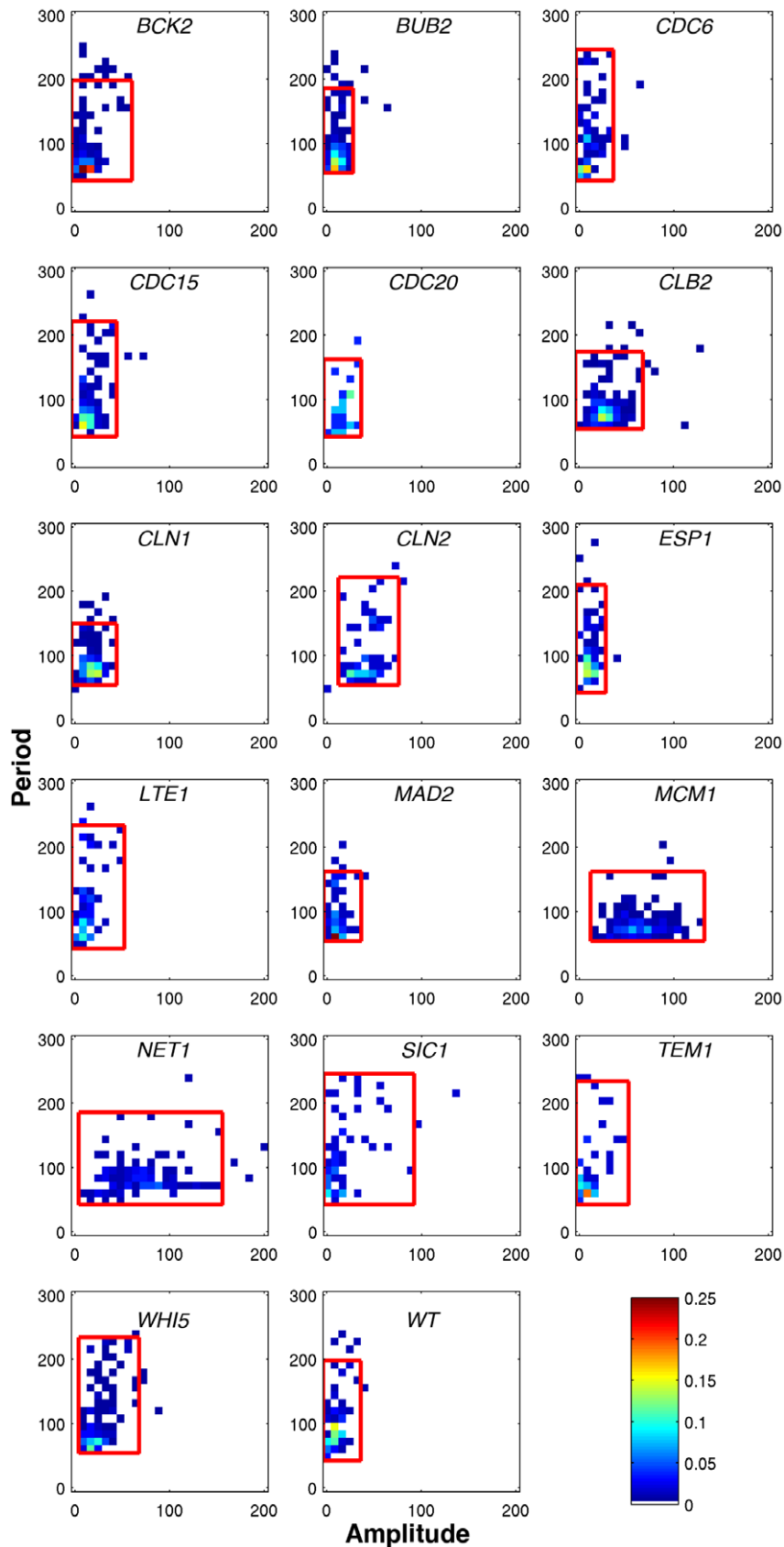
Figure 4. Distributions of amplitude and period estimates for gene expression for 16 GFP-tagged strains and WT. Red boxes enclose 95% of all cells. Low-pass Butterworth filtering removes all oscillations with non-physiological periods, which leaves only periods greater than 50 min. Using a t-test, we compared the amplitude distribution (x-axis) for each strain with that of wild-type (wt) cells to determine if the protein level

exhibits noticeable oscillations. The color of each bin represents the fraction of cell cycles that fall in that bin, indicated by the colorbar in the lower right.

as oscillatory at the protein level also exhibit transcriptional oscillations (*CLB2, CLN1, CLN2, SIC1,* and *WHI5*). The peak in protein fluorescence coincides with the reported peak in mRNA level for *CLN1, CLN2,* and *WHI5,* but not for *CLB2* and *SIC1*. However, three of the genes oscillating at the protein level (*CDC15, MCM1,* and *NET1*) are not oscillating at the transcriptional level.

For many of these proteins, time-courses of protein expression have been previously characterized by Western blots of synchro-
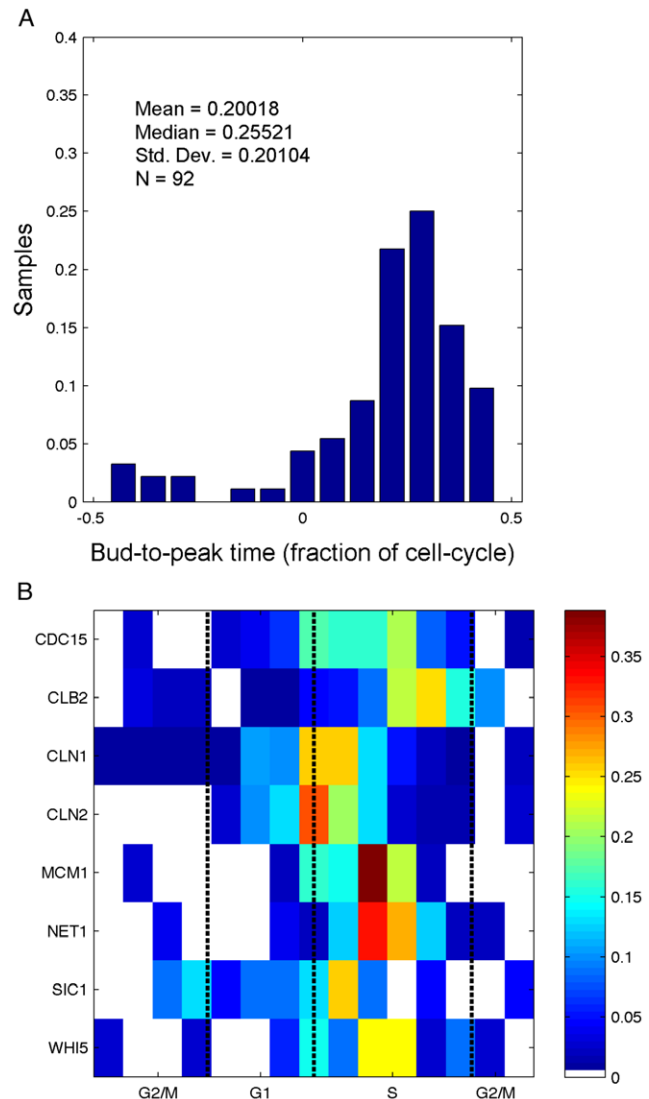

Figure 5. Phase of peak expression in cell-cycle normalized time. (A) Distribution of the time between bud emergence and peak fluorescence for the CLB2-GFP strain. (B) Distributions of all GFP-tagged strains, with color representing fraction of cells comparable to the height of each bin displayed in (A). Cell-cycle stages are based on the relative length of each stage from [26], and assuming that bud emergence occurs at the G1-S transition. The boundaries between the different stages are represented by the dashed vertical lines. Because of the difficulty in identifying all budding events, the bud-to-peak time value is found by locating the closest peak in the fluorescence time-course to each identified budding event.

nized cultures. Bck2 fluctuations during the yeast cell cycle have not been much studied; our results indicate that it is not a periodic protein. Similar to the single cell data presented here, Fraschini et al found the abundance of Bub2 to be constant during the 150 minutes following release from α-factor block in G1 [30]. Cdc6 was shown to be high in late M and early G1, and low otherwise [31]. Although we did not observe this in single plane fluorescence measurements, a similar pattern was observed in the z-stack reported in Figure 3. Jaspersen et al demonstrated that Cdc15 abundance is constant through the cell cycle after α-factor synchronization [32]. In contrast, we found the fluctuations in Cdc15-GFP fluorescence to be significantly different from that of untagged cells. Clb2 is known to peak in abundance at mitosis [33] but in our experiments, we find the peak fluorescence of Clb2-GFP to occur in late S phase. Tyers et al showed that Cln1 and Cln2 reach their peak abundances just after START [34], which is consistent with the observations presented here. Esp1 is another protein whose abundance is known to oscillate, with a distinct trough in G1 phase [35]. However, any fluorescence fluctuations in the ESP1-GFP strain were insignificant when compared to untagged cells. Our observations of GFP-tagged strains are consistent with literature reports that protein abundance is constant for Lte1 [36] and for Mad2 [37]. Mcm1 is reported to be non-oscillatory at the transcriptional level [29] but no reference reporting the evolution of protein abundance could be found. Our data shows that Mcm1 is always highly localized in the nucleus, and we see clear evidence of a sharp drop in mean fluorescence around the time of cell division The abundance of Net1 was measured to be constant throughout the cell cycle [38]. However, we see clear oscillations that peak, on average, in S phase. Sic1 abundance peaks in G1 and decreases at START [39]. We observe clear oscillations in Sic1-GFP fluorescence but at a later stage, shortly after START. The abundance of Tem1 is low in G1 and early S phases, begins to accumulate in M phase, and peaks during telophase [36] but our observations of fluctuations in Tem1-GFP fluorescence are indistinguishable from untagged cells. The visual inspection of images of GFP-tagged Whi5 did not reveal any obvious oscillation of protein abundance [40]. Our data set is consistent with these results as oscillations of GFP-tagged Whi5 are mild and barely detectable by visual inspection (Figure 2). However, the statistical analysis of the dataset uncovered evidence of oscillations peaking in S phase (Figure 5B). In agreement with the results of [40], we see that Whi5 is strongly localized in the nucleus in G1 phase (Figure 3). The relative expression of Sic1 and Whi5 (Figure 5B) also appears consistent with the results reported by Constanzo [40].

Discussion

It is natural to compare the results presented in this report with current models describing the function, localization, and expression dynamics of the proteins studied in these experiments.

The set of genes analyzed here were chosen according to several criteria. In order to make a broad assessment of the effects of noise on cell cycle progression, we wanted to include in the experimental design as many cell cycle genes as practical. To ensure consistency and reproducibility, we chose to use GFP-tagged strains from an existing library. Some genes important for cell cycle regulation are not available in the library (e.g., *CLN3, CLB5, SWE1*). The genotype of the *CDC14-GFP* and *SWI5-GFP* strains indicate that

Table 3. Phase of fluorescence signal with respect to bud emergence, and comparison with mRNA peak.

Protein	Mean Protein Peak (fraction of cell cycle)	mRNA Peak [27] (fraction of cell cycle)	Difference
Cdc15	0.098	N/A	N/A
Clb2	0.200	0.410	−0.210
Cln1	0.025	0.000	0.025
Cln2	0.031	−0.030	0.061
Mcm1	0.103	N/A	N/A
Net1	0.151	N/A	N/A
Sic1	−0.032	−0.210	0.178
Whi5	0.119	0.090	0.029

doi:10.1371/journal.pone.0026272.t003

the GFP tag is probably inserted in a different genomic location. We have therefore excluded these two important strains from this report.

It is important to remember that the criterion used to detect oscillations of protein abundance is based on a statistical comparison with the observed fluctuations of cell autofluorescence throughout the cell division cycle. As a result, for those proteins that show no evidence of periodicity by this criterion (namely, Bck2, Bub2, Cdc6, Esp1, Lte1, Mad2, and Tem1) it is not possible to decide whether they are present at constant levels throughout the cell cycle or oscillate with amplitudes smaller than the cell autofluorescence. The low levels of fluorescence that we observe for these GFP-tagged cell cycle proteins are actually puzzling. The weak signals may reflect the low abundances of these proteins. It is also possible that in some of the strains, the fluorescent domain is degraded rapidly compared to its maturation time because of the rapid turnover of the protein to which it is attached.

Our fluorescence measurements might also be confounded by organelle motion, which, by carrying localized tagged proteins in to and out of the plane of focus, could generate fluctuations that appear uncorrelated with the cell cycle (and most likely removed by the low-pass filtering). Cdc6 is a clear example of this phenomenon: no oscillations were discernible in the single plane measurements, but maximum z-projection data (Figure 3) demonstrate clearly that Cdc6 total abundance and spatial localization both oscillate during the cell cycle.

It is interesting to note that for the proteins that we observe as oscillatory (Clb2, Cln1, Cln2, Cdc15, Sic1, and Whi5), the periods and amplitudes have larger CVs than that of the inter-bud times (Table 2). This suggests that the cell-cycle control mechanism is buffered so that the timing of bud emergence and cell division is less noisy than the periodic fluctuations of individual components of the underlying control mechanism.

Net1 and Mcm1 are special cases because their mean fluorescence oscillates strongly during the cell cycle but at the same time they remain confined to specific cellular compartments, the nucleolus for Net1 and the nucleus for Mcm1. They call for establishing a distinction between protein abundance in concentration and total amount. Proteins that remain at a constant concentration through the cell cycle double in amount over one cell cycle period. When proteins are uniformly distributed in the cell, the protein concentration is well approximated by the average fluorescence of a sufficiently larger number of pixels. As a result, they are fairly insensitive to the limitations of the image segmentation algorithm. When a protein is localized in a small fraction of the cell volume, estimating the time-evolution of the concentration requires the division of the cell total fluorescence by

an estimate of the cell volume, something that the image segmentation algorithm does not provide. Because the segmentation tends to delimit the contour of the mother cell and ignore the bud, the number of pixels used to average the fluorescence remains fairly constant throughout the cell cycle. Hence, the mean fluorescence measurement corresponds to the average concentration of Mcm1 (and Net1) in the mother portion of the cell (where the nucleus resides until nuclear division [41]), and the oscillations observed for Net1 and Mcm1 may reflect a doubling in amount in the mother cell, not necessarily in concentration averaged across mother and daughter. This interpretation could explain the discrepancy between data obtained by bulk measurement and by imaging. When we divide total fluorescence by total number of pixels in mother cell + bud (data not shown), we find that the oscillations in mean fluorescence of Net1 and Mcm1 are damped but not eliminated.

More fundamentally, it is not clear if average concentrations or total amounts are better indicators of biological activity. The notion of cellular concentration of a compound that remains confined to a very small fraction of the cell volume does not seem relevant. On the contrary, the possibility to combine localization and abundance data, as it is possible by imaging cytometry, may be a better telltale of protein dynamics than more traditional bulk measurements.

More generally, it is important to keep in mind that the relationship between protein abundance and fluorescence measurements remains poorly characterized *in vivo*. Very little information is available about the maturation and degradation rates of fluorescent proteins *in vivo*. It is not clear how these parameters are altered by fusion to another protein. It is also possible that the addition of the ~27 kDa GFP moiety to the C-terminus of a cell cycle regulating protein may interfere with its function, as may be the case for Cdc20 and Sic1.

Contrary to more conventional measurement techniques that require extraction of proteins and RNAs from bulk cultures, time-lapse microscopy does not require synchronizing cells. It is therefore likely that the single cell measurements reported here better reflect the natural progression of the cell cycle than bulk measurements of synchronized cells that were used in the past. Not only could the synchronization process interfere with the cell cycle, but also bulk measurements could mask how each cell behaves throughout the division process. Also we are measuring a proxy for protein abundance, whereas other efforts to globally observe gene expression have focused mainly on transcription and mRNA levels [28,29]. In order to gain a more comprehensive picture of cell cycle dynamics, future studies should combine single-cell measurement of mRNA [42] with single-cell proteomic data. Labeling

multiple cell cycle genes with optically separable reporters would make it possible to estimate the correlation between the expression levels of different proteins.

Materials and Methods

Yeast Strains and Media

Each *S. cerevisiae* strain used in this study included GFP inserted as a C-terminal fusion downstream of a protein involved in cell-cycle control as described in [43]. All strains were purchased from Invitrogen (Carlsbad, CA).

All experiments were conducted using synthetic complete (SC) growth medium with 2% glucose at 30°C. Cell cultures were grown overnight from glycerol stocks, and prior to microscopic observation, the cells were verified to be in the exponential growth phase by measuring the OD_{600}. Small volumes (~3 µL) of liquid culture were added to a #1.5 microscope coverslip, and covered with a thin SC agar slab to limit cell motion.

Genotyping

To verify the genotypes of the individual strains, they were first streaked on histidine dropout agar plates, colonies were selected and the genomic DNA extracted using the purelink™ genomic DNA extraction kit (Invitrogen, Carlsbad, CA) according to the manufacturer's instructions. The genomic DNA was then genotyped by polymerase chain reaction (PCR) using the corresponding CHK and R1 primer pairs from Huh et al. [43] in a master mix containing 1× HotStarTaq DNA polymerase master mix (Qiagen,Valencia, CA) and 1.6 µM each primer in 30 µL volume. The amplification program was the following: 95 C for 1 min; 95 C for 30 s, 51 C for 30 s, 72 C for 2 min repeat 35×; 72 C for 10 min. The results were analyzed by agarose gel electrophoresis. The genotype is confirmed by a 2.8 kb band corresponding to the cassette GFPS65T-HIS3MX6 inserted at the expected genomic locus, whereas a band of 0.5 kb to 0.65 kb indicates a WT locus and the presence of the GFPS65T-HIS3MX6 cassette somewhere else in the genome.

Fluorescence Microscopy

All images were collected on a DeltaVision microscope (Applied Precision, LLC, Issaquah, WA), which is equipped with an LED lamp for bright-field mode, and a 250 W Xenon lamp for fluorescence excitation. The DeltaVision has automated components, including the x-y-z translation stage, filter wheels, shutters, and is equipped with a CoolSNAP HQ camera (Photometrics, Tucson, AZ). A 60× phase contrast objective was used to collect both phase contrast and fluorescence images. A GFP filter-set with the excitation band centered at 470 nm (full-width of 40 nm) and emission band centered at 525 nm (full-bandwidth of 50 nm) was used to image GFP-expressing cells with an exposure time of 100 ms. Images were collected from 20 different regions for each cell line at 5-minute intervals for a total of 5 hours or until cell density became too great to permit identification. No significant photobleaching was observed in this period of time under these illumination conditions. The optimal focal plane for each region was found using the DeltaVision's built-in autofocus function in the Phase-contrast channel prior to collection of each time-point.

To ensure that the observed changes in localized concentration were not an artifact from an organelle moving in and out of focus, three-dimensional stacks consisting of 21 z-sections were obtained for each cell with a z-step size of 0.5 µm using the DeltaVision control software softWorx and the same filters and exposure times described above. Only 5 regions from each cell line could be observed with these conditions, due to the increased number of

focal planes collected. We also noticed that the cells exhibited much longer inter-division times, which we believe is due to the increased amount of light exposure. Cell strains that did not contain GFP did not grow at all under these conditions (data not shown).

Movies of oscillating genes (Cln2 and Net1) are included in the online supplement (Movies S1, S2, S3, and S4). All images collected in the context of this work are available at https://sirion. vbi.vt.edu/yeast_GFP_data/.

Image Processing

Phase-contrast images are segmented using custom software derived from Yeast Tree 1.6.3 [14]. The application relies on the MATLAB Image Processing toolbox. First, the function 'imfill' is used to flood-fill local minimum not connected to the image border, which fills in the center of the groups of cells. As each group of cells will have slightly different levels to which the flood-fill will rise, we then search the image histogram for intensities greater than the calculated background, taken from the border pixels, and with a frequency greater than the minimum cell area, generally set to 200 pixels. To keep only large groups of connected pixels, an erosion (built-in function 'imerode') is performed, removing the outermost pixels of a region and eliminating small groups of pixels.

The next step is to separate these groups into individual cells. This is done with another call to 'imerode' to cut the small necks that appear between touching cells. Once the cells are cut, the remaining connected regions are labeled with a call to the built-in function 'bwlabel', which identifies the individual cells and assigns each with a unique label. To finish, the cells are returned to their original sizes with a dilation (built-in function 'imdilate'), which adds pixels around the edges of each cell.

After all frames in the time-series are segmented, the pixels making up each cell body are mapped to the previous frame by calculating the overlap (defined here as the ratio of the intersection of cell-body pixels to their union) of the current cell with the cells in the previous frame.

The three-dimensional stacks used for calculating localized concentration were reduced to 2D images by use of the maximum Z projection in MATLAB.

The image processing software used in this work is available in the online supplement (Software S1).

Data analysis

In an effort to determine if each protein was oscillating with the cell cycle, we used spectral subtraction to remove noise [44]. Briefly, the mean noise spectrum, $\mu(f)$, is calculated by averaging the magnitudes of all wild type cells' Fourier spectra. For each cell of the 17 strains, an individualized filter, $H(f)$, is then constructed such that

$$H(f) = 1 - \frac{\mu(f)}{|X(f)|}$$

where $|X(f)|$ is the magnitude of the Fourier transform, $X(f)$ of the cell's time-course. The Fourier spectrum is then multiplied by the filter, and the inverse Fourier transform is taken to obtain the filtered time-domain data.

The resulting trajectories still contain high-frequency noise, as well as non-zero mean, so the individual cell trajectories are then de-trended by subtracting out the best-fit straight line from the time-course, and filtered using a low-pass Butterworth filter with a cut-off frequency set to 0.333 mHz (corresponding to a period of

50 min). The Butterworth filter is constructed such that the attenuation at the cut-off frequency is 3 dB. Peaks in the filtered data were then found by first locating local extrema, with the criteria that each peak (trough) must have a value $>$ ($<$) 10% of the global maximum (minimum) for that cell, and that each pair of consecutive peaks (troughs) must be separated by 1 trough (peak). The period (in minutes) of each cycle was then estimated as the time between consecutive peaks, while the amplitude of each cycle was calculated as the difference between the first peak and the subsequent trough in that cycle.

The distribution of peak-to-peak times for each cell-line has been visualized in several ways. The 2-D histograms consist of 20 bins for each parameter. To obtain the boxes representing the 95th percentile of cycles, we start by counting the number of cycles that fall into the bin representing the mean parameter values of the population. This box is then expanded 1 bin in each direction until 95% of the cells are contained in the box.

The standard deviation of the mean peak-to-peak time was calculated for each cell, in order to compare the variability from one cell cycle to the next in a single cell to the variability from cell to cell.

After applying the low-pass filter, all cells exhibit oscillation periods with mean values that are biologically feasible and the distributions of periods for proteins that are known to oscillate are not significantly different from the untagged (wild-type) strain. However the distributions of amplitudes for the various genes (Figure 4) are highly variable. Even the autofluorescence of the wild-type strain with no GFP tag shows low-amplitude oscillations (mean amplitude = 26 a.u., max amplitude less than ~80 a.u.). To identify oscillatory proteins, we compared the amplitude distribution of each strain to the wild-type cells with a 2-sample, unequal variance t-test. At the 1% significance level, the amplitude distributions of following proteins could not have originated from the wild-type distribution: Cdc15, Clb2, Cln1, Cln2, Mcm1, Net1, Sic1, and Whi5.

Protein localization was quantified by first locating the pixel, P_{max}, exhibiting the maximum fluorescence intensity, I_{max}, within

a given cell. Then each of the 8 pixels neighboring P_{max} was evaluated for whether its intensity was within the top 5% of the brightest pixels within the cell. If so, this pixel was added to the set containing P_{max}. Then the nearest neighbors of the extended set were evaluated in like manner, until the set could be extended no further (or until the cell border was reached).

Supporting Information

Appendix S1   Assessment of data analysis algorithms on non-oscillating simulated cells.
(PDF)

Movie S1   Movie derived from Cln2 images (.mov format).
(MOV)

Movie S2   Movie derived from Cln2 images (.avi format).
(AVI)

Movie S3   Movie derived from Net1 images (.mov format).
(MOV)

Movie S4   Movie derived from Net1 images (.avi format).
(AVI)

Software S1   Image analysis software.
(TAR)

Acknowledgments

Author Contributions

Conceived and designed the experiments: JP DB JT. Performed the experiments: DB JM MP. Analyzed the data: DB WB JT KC JP. Wrote the paper: DB KC WB JP JT.

References

1. Morgan DO (2007) The cell cycle : principles of control. London: New Science Press, Ltd.
2. Barik D, Baumann WT, Paul MR, Novak B, Tyson JJ (2010) A model of yeast cell-cycle regulation based on multisite phosphorylation. Mol Syst Biol 6: 405.
3. Kar S, Baumann W, Paul M, Tyson JJ (2009) Exploring the roles of noise in the eukaryotic cell cycle. Proc Natl Acad Sci USA.
4. Ball DA, Ahn T-H, Wang P, Chen KC, Cao Y, et al. (2011) Stochastic exit from mitosis in budding yeast: model predictions and experimental observations. Cell Cycle 10: 999–1009.
5. Chen KC, Calzone L, Csikasz-Nagy A, Cross FR, Novak B, et al. (2004) Integrative analysis of cell cycle control in budding yeast. Molecular Biology of the Cell 15: 3841–3862.
6. Cooper S (2004) Is whole-culture synchronization biology's 'perpetual-motion machine'? Trends Biotechnol 22: 266–269.
7. Cooper S (2004) Rejoinder: whole-culture synchronization cannot, and does not, synchronize cells. Trends Biotechnol 22: 274–276.
8. Spellman PT, Sherlock G (2004) Reply: whole-culture synchronization - effective tools for cell cycle studies. Trends Biotechnol 22: 270–273.
9. Spellman PT, Sherlock G (2004) Final words: cell age and cell cycle are unlinked. Trends Biotechnol 22: 277–278.
10. Raser J, O'Shea EK (2004) Control of stochasticity in eukaryotic gene expression. Science 304: 1811–1814.
11. Elowitz MB, Levine A, Siggia ED, Swain P (2002) Stochastic gene expression in a single cell. Science 297: 1183–1186.
12. Cormack BP, Bertram G, Egerton M, Gow NA, Falkow S, et al. (1997) Yeast-enhanced green fluorescent protein (yEGFP)a reporter of gene expression in Candida albicans. Microbiology (Reading, Engl) 143(Pt 2): 303–311.
13. Sigal A, Milo R, Cohen A, Geva-Zatorsky N, Klein Y, et al. (2006) Variability and memory of protein levels in human cells. Nature 444: 643–646.
14. Bean JM, Siggia ED, Cross FR (2006) Coherence and timing of cell cycle start examined at single-cell resolution. Molecular Cell 21: 3–14.
15. Cross FR, Schroeder L, Bean JM (2007) Phosphorylation of the Sic1 inhibitor of B-type cyclins in Saccharomyces cerevisiae is not essential but contributes to cell cycle robustness. Genetics 176: 1541–1555.
16. Di Talia S, Skotheim JM, Bean JM, Siggia ED, Cross FR (2007) The effects of molecular noise and size control on variability in the budding yeast cell cycle. Nature 448: 947–951.
17. Gordon A, Colman-Lerner A, Chin T, Benjamin K, Yu R, et al. (2007) Single-cell quantification of molecules and rates using open-source microscope-based cytometry. Nat Meth 4: 175–181.
18. Charvin G, Cross FR, Siggia ED (2008) A microfluidic device for temporally controlled gene expression and long-term fluorescent imaging in unperturbed dividing yeast cells. PLoS ONE 3: e1468.
19. Skotheim JM, Di Talia S, Siggia ED, Cross FR (2008) Positive feedback of G1 cyclins ensures coherent cell cycle entry. Nature 454: 291–296.
20. Drapkin BJ, Lu Y, Procko AL, Timney BL, Cross FR (2009) Analysis of the mitotic exit control system using locked levels of stable mitotic cyclin. Mol Syst Biol 5: 328.
21. Ikui AE, Cross FR (2009) Specific genetic interactions between spindle assembly checkpoint proteins and B-Type cyclins in Saccharomyces cerevisiae. Genetics 183: 51–61.
22. Lu Y, Cross FR (2009) Mitotic exit in the absence of separase activity. Molecular Biology of the Cell 20: 1576–1591.
23. Tully GH, Nishihama R, Pringle JR, Morgan DO (2009) The anaphase-promoting complex promotes actomyosin-ring disassembly during cytokinesis in yeast. Molecular Biology of the Cell 20: 1201–1212.
24. Charvin G, Oikonomou C, Siggia ED, Cross FR (2010) Origin of irreversibility of cell cycle start in budding yeast. PLoS Biol 8: e1000284.
25. Lu Y, Cross FR (2010) Periodic cyclin-Cdk activity entrains an autonomous Cdc14 release oscillator. Cell 141: 268–279.
26. Brewer BJ, Chlebowicz-Sledziewska E, Fangman WL (1984) Cell cycle phases in the unequal mother/daughter cell cycles of Saccharomyces cerevisiae. Molecular and Cellular Biology 4: 2529–2531.

27. Gauthier NP, Jensen LJ, Wernersson R, Brunak S, Jensen TS (2010) Cyclebase.org: version 2.0, an updated comprehensive, multi-species repository of cell cycle experiments and derived analysis results. Nucleic Acids Res 38: D699–702.

28. Pramila T, Wu W, Miles S, Noble WS, Breeden LL (2006) The Forkhead transcription factor Hcm1 regulates chromosome segregation genes and fills the S-phase gap in the transcriptional circuitry of the cell cycle. Genes Dev 20: 2266–2278.

29. Spellman PT, Sherlock G, Zhang MQ, Iyer VR, Anders K, et al. (1998) Comprehensive identification of cell cycle-regulated genes of the yeast Saccharomyces cerevisiae by microarray hybridization. MolBiolCell 9: 3273–3297.

30. Fraschini R, Formenti E, Lucchini G, Piatti S (1999) Budding yeast Bub2 is localized at spindle pole bodies and activates the mitotic checkpoint via a different pathway from Mad2. J Cell Biol 145: 979–991.

31. Piatti S, Lengauer C, Nasmyth K (1995) Cdc6 is an unstable protein whose de novo synthesis in G1 is important for the onset of S phase and for preventing a 'reductional' anaphase in the budding yeast Saccharomyces cerevisiae. EMBO J 14: 3788–3799.

32. Jaspersen SL, Charles JF, Tinker-Kulberg RL, Morgan DO (1998) A late mitotic regulatory network controlling cyclin destruction in Saccharomyces cerevisiae. Molecular Biology of the Cell 9: 2803–2817.

33. Grandin N, Reed SI (1993) Differential function and expression of Saccharomyces cerevisiae B-type cyclins in mitosis and meiosis. Molecular and Cellular Biology 13: 2113–2125.

34. Tyers M, Tokiwa G, Futcher B (1993) Comparison of the Saccharomyces cerevisiae G1 cyclins: Cln3 may be an upstream activator of Cln1, Cln2 and other cyclins. EMBO J 12: 1955–1968.

35. Jensen S, Segal M, Clarke DJ, Reed SI (2001) A novel role of the budding yeast separin Esp1 in anaphase spindle elongation: evidence that proper spindle association of Esp1 is regulated by Pds1. J Cell Biol 152: 27–40.

36. Bardin AJ, Visintin R, Amon A (2000) A mechanism for coupling exit from mitosis to partitioning of the nucleus. Cell 102: 21–31.

37. Chen RH, Brady DM, Smith D, Murray AW, Hardwick KG (1999) The spindle checkpoint of budding yeast depends on a tight complex between the Mad1 and Mad2 proteins. Molecular Biology of the Cell 10: 2607–2618.

38. Azzam R, Chen SL, Shou W, Mah AS, Alexandru G, et al. (2004) Phosphorylation by cyclin B-Cdk underlies release of mitotic exit activator Cdc14 from the nucleolus. Science (New York, NY) 305: 516–519.

39. Donovan JD, Toyn JH, Johnson AL, Johnston LH (1994) P40SDB25, a putative CDK inhibitor, has a role in the M/G1 transition in Saccharomyces cerevisiae. Genes Dev 8: 1640–1653.

40. Costanzo M, Nishikawa JL, Tang X, Millman JS, Schub O, et al. (2004) CDK activity antagonizes Whi5, an inhibitor of G1/S transcription in yeast. Cell 117: 899–913.

41. Hartwell LH, Culotti J, Reid B (1970) Genetic control of the cell-division cycle in yeast. I. Detection of mutants. Proc Natl Acad Sci USA 66: 352–359.

42. Zenklusen D, Larson DR, Singer RH (2008) Single-RNA counting reveals alternative modes of gene expression in yeast. Nat Struct Mol Biol 15: 1263–1271.

43. Huh WK, Falvo JV, Gerke LC, Carroll AS, Howson RW, et al. (2003) Global analysis of protein localization in budding yeast. Nature 425: 686–691.

44. Boll SF (1979) Suppression of Acoustic Noise in Speech Using Spectral Subtraction. Ieee Transactions on Acoustics Speech and Signal Processing 27: 113–120.

45. Cherry JM, Adler C, Ball C, Chervitz SA, Dwight SS, et al. (1998) SGD: Saccharomyces Genome Database. Nucleic Acids Res 26: 73–79.

46. Ghaemmaghami S, Huh W-K, Bower K, Howson R, Belle A, et al. (2003) Global analysis of protein expression in yeast. Nature 425: 737–741.

47. Pereira G, Höfken T, Grindlay J, Manson C, Schiebel E (2000) The Bub2p spindle checkpoint links nuclear migration with mitotic exit. Molecular Cell 6: 1–10.

48. Piatti S, Böhm T, Cocker JH, Diffley JF, Nasmyth K (1996) Activation of S-phase-promoting CDKs in late G1 defines a "point of no return" after which Cdc6 synthesis cannot promote DNA replication in yeast. Genes Dev 10: 1516–1531.

49. Ciosk R, Zachariae W, Michaelis C, Shevchenko A, Mann M, et al. (1998) An ESP1/PDS1 complex regulates loss of sister chromatid cohesion at the metaphase to anaphase transition in yeast. Cell 93: 1067–1076.